Electronic structure of Cu_2ZnSnS_4 probed by soft x-ray emission and absorption spectroscopy

M. Bär,[1,*] B.-A. Schubert,[1] B. Marsen,[1] S. Schorr,[1,2] R. G. Wilks,[1] L. Weinhardt,[3] S. Pookpanratana,[4] M. Blum,[4] S. Krause,[4] Y. Zhang,[4] W. Yang,[5] T. Unold,[1] C. Heske,[4] and H.-W. Schock[1]

[1]*Solar Energy Research, Helmholtz-Zentrum Berlin für Materialien und Energie GmbH (HZB), Hahn-Meitner-Platz 1, D-14109 Berlin, Germany*

[2]*Freie Universität Berlin, Department of Geosciences, Malteser Str. 74-100, D-12249 Berlin, Germany*

[3]*Exp. Physik VII, Universität Würzburg, Am Hubland, D-97074 Würzburg, Germany*

[4]*Department of Chemistry, University of Nevada, Las Vegas, 4505 Maryland Pkwy., Las Vegas, Nevada 89154, USA*

[5]*Advanced Light Source (ALS), Lawrence Berkeley National Laboratory, 1 Cyclotron Rd., Berkeley, California 94720, USA*

(Received 19 April 2011; revised manuscript received 9 June 2011; published 25 July 2011)

The electronic structure of Cu_2ZnSnS_4 has been investigated by S $L_{2,3}$ x-ray emission and absorption spectroscopy. An empirical assignment of the most prominent spectral features of the valence and conduction band, respectively, can be made based on a comparison with spectra of corresponding binary compounds and with calculated densities of states. We find that the top of the valence band is dominated by hybridized *antibonding* Cu 3d-S 3p states, while the bottom of the conduction band is dominated by respective Sn 5s-S 3p states. We also determine the electronic band gap near the Cu_2ZnSnS_4 surface to be 1.5 (±0.3) eV.

DOI: 10.1103/PhysRevB.84.035308 PACS number(s): 73.61.Le, 78.70.Dm, 78.70.En

I. INTRODUCTION

$Cu_2ZnSn(S,Se)_4$ kesterites composed of earth-abundant elements have recently become the focus of significant research efforts. They not only represent a complex semiconductor materials class that, through deliberate compositional variation, allows access to a vast region of parameter space,but also have also shown great promise as an alternative material system for thin-film solar cell absorbers.[1–7] From both perspectives, a detailed insight into the electronic structure of kesterites is necessary. However, so far the electronic structure of the $Cu_2ZnSn(S,Se)_4$ material system has only been thoroughly investigated in theoretical studies,[8–11] while an experimental analysis is still lacking. One reason for this deficit is, presumably, the complex (structural) phase diagram of the Cu-Zn-Sn-S-Se system[12,13] and related problems to deposit high-quality material free of impurity and/or mixed crystal phases. Recently, we have been able to synthesize Cu_2ZnSnS_4 ("CZTS") powder and thin-film samples and to demonstrate that they consist of single-phase stoichiometric Cu_2ZnSnS_4 material (i.e., no impurity phases could be detected) crystallized in a kesterite structure[14,15]. Since the four nearest neighbors of an S atom in a CZTS *kesterite* are always two Cu, one Zn, and one Sn[8,9] and because of the expected hybridization of S 3p states with Zn, Sn, and Cu states,[16] we have used S $L_{2,3}$ x-ray emission (XES) and absorption (XAS) spectroscopy to determine the electronic structure of these well-defined CZTS materials. Note that while XES is probing occupied states (including the valence band), XAS is probing unoccupied states (including the conduction band), and thus their combination can also give information about the band gap of the probed material. By focusing on the S $L_{2,3}$ edge, it is possible to elucidate the local chemical environment around the S atoms, which, in turn, gives deep insight into the chemical bonding between sulfur and the metal constituents of CZTS. In this paper, the experimental electronic structure (valence *and* conduction bands) will be elucidated by comparison of respective CZTS spectra with the spectra of related binary compounds and with calculated density of states (DOS) using density functional theory (DFT).[8,9]

II. EXPERIMENTAL

The investigated CZTS powder was synthesized in a solid-state reaction of a stoichiometrically weighted Cu_2SnS_3 + ZnS mixture by annealing in an evacuated quartz ampoule at 720 °C.[14] *In situ* x-ray diffraction measurements show the formation of stoichiometric CZTS without any detectable (crystalline) impurity phases.[14] Polycrystalline CZTS thin films (∼1.5 μm thick) were deposited at the HZB on Mo-coated soda-lime glass using thermal coevaporation of zinc sulfide, copper, and tin source materials in a Cu-rich process (see Ref. 15 for more details). Chemical analysis by energy-dispersive x-ray spectroscopy confirms that the obtained CZTS films are stoichiometric. As reference samples, commercially available powders (Alfa Aesar, purity >99%) of the respective binaries (Cu_2S, CuS, ZnS, SnS, and SnS_2) were investigated. The CZTS thin films were subjected to a KCN etch (1.5 M aqueous solution for 3 min) in order to ensure the removal of any Cu_xS phases from the surface. After etching, the samples were packed under dry nitrogen to minimize air exposure and transported to the ALS for characterization. All samples were analyzed by XES and XAS at Beamline 8.0.1 of the ALS using the soft x-ray fluorescence endstation.[17] The energy scale of the S $L_{2,3}$ XES spectra was calibrated using a CdS reference spectrum.[18] A common energy scale for the XES and XAS measurements was established by measuring several elastically scattered (Rayleigh) lines of different excitation energy. The XAS spectra were measured in partial fluorescence yield (PFY) mode using the XES spectrometer (gated such that the Rayleigh line did not influence the measurement). Both, XES and (PFY) XAS probe the electronic structure near the sample surface—for the photon energies involved in our S $L_{2,3}$ XES and XAS measurements and assuming a CZTS density

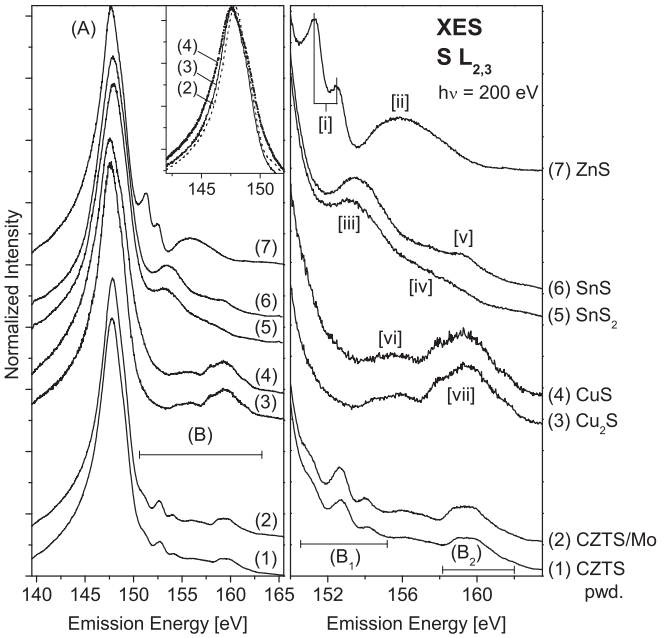

FIG. 1. S $L_{2,3}$ XES spectra (left: overview; right: region (B) on an expanded energy scale) of CZTS samples and related binary compounds. Region (A) of the S $L_{2,3}$ emission for samples (2)–(4) is compared in the inset of the left panel.

of 4.6 g/cm^3, the 1/e attenuation lengths are estimated to be 23 and 20 (±1) nm, respectively.[19]

III. RESULTS

Figure 1 (left) shows the S $L_{2,3}$ XES spectra of two CZTS samples [powder ("CZTS pwd.," 1) and thin film ("CZTS/Mo," 2)] and related binary compounds (3–7), non-resonantly excited at 200 eV. As is well-known for sulfide S $L_{2,3}$ XES spectra,[16,18,20] we find a dominant emission at ∼147.5–148.0 eV (A). This peak is attributed to transitions (i.e., radiative decay) of electrons from S 3s-derived electronic states into the spin-orbit-split S $2p_{1/2}$ and $2p_{3/2}$ core holes, resulting in S L_2 and L_3 emission, respectively. Due to the spin-orbit splitting of the S 2p core state (∼1.2 eV for sulfides[21]), the width of the S 3s band,[22] and the lifetime broadening of the S 3s valence-hole state,[18,23] the splitting between L_2 and L_3 emission manifests itself only in an asymmetry of the S 3s line at higher emission energies. The emission in region (B) (150–163 eV) is due to transitions from shallower valence states. The details of this region are shown on an expanded energy scale in Fig. 1 (right). In order to understand the spectral shape of the S $L_{2,3}$ (valence) emission of the CZTS samples and hence the electronic structure of the valence band, we first focus on the spectra of the most closely related binary compounds, namely Cu_2S, ZnS, and SnS_2. Furthermore, since CuS and SnS could be present as secondary impurity phases, the corresponding spectra are also considered and shown for reference. In the well-known S $L_{2,3}$ XES spectrum of ZnS, two very distinct features [i] at 151.3 and 152.5 eV and a broad emission [ii] between 153.8 and 159.8 eV are observed. While features [i] are due to transitions from Zn 3d-derived states, emission [ii] stems from electrons in the upper valence band (Zn 4s-S 3p hybridized states) decaying into the S 2p core holes[16,24]—a summary of the spectral features discussed here and their attribution to different electronic states is given in Table I. Analogous to the Cd 4d-derived states in the S $L_{2,3}$ XES spectrum of CdS,[16] the here-considered Zn 3d-derived states are expected to exhibit a smaller life-time broadening than the S 3s states, which explains why the L_2 and L_3 emission from the Zn 3d-related states give rise to two well-separated features [i].

The S $L_{2,3}$ XES spectra of the two tin sulfides show a pronounced emission feature [iii] at 153.6 eV, accompanied by a broad shoulder [iv] between 156 and 160 eV. Based on a comparison with DFT calculations,[25] these emission features can be ascribed to transitions of electrons from hybridized *bonding* Sn 5s-S 3p and Sn 5p-S 3p states, respectively. Furthermore, the SnS spectrum deviates from that of SnS_2 by an additional feature [v] at 159.3 eV. As proposed by Ref. 26, we interpret feature [v] as indicative of the coupling of Sn 5p with hybridized *antibonding* Sn 5s-S 3p states. Photoemission experiments[27] and band structure calculations[25,28] suggest that the reason for the presence of feature [v] is related to a reduced energy difference between hybridized *bonding* and *antibonding* Sn 5s-S 3p states. While

TABLE I. Summary of the spectral features and their attribution to specific electronic states.

Spectral feature	Compound	Ascribed to	Refs.
(A) XES S $L_{2,3}$	Sulfides	S 3s-derived states	16, 18, 20
(B) XES S $L_{2,3}$	Sulfides	Valence band states	16, 18, 20
[i] XES S $L_{2,3}$	ZnS	Zn 3d-derived states	16, 24
[ii] XES S $L_{2,3}$	ZnS	Hybridized (Zn 4s-S 3p) states	16, 24
[iii] XES S $L_{2,3}$	SnS, SnS_2	Hybridized (Sn 5s-S 3p) states	25
[iv] XES S $L_{2,3}$	SnS, SnS_2	Hybridized (Sn 5p-S 3p) states	25
[v] XES S $L_{2,3}$	SnS, SnS_2	Hybridized (Sn 5s-S 3p)[a] states	25,26
[vi] XES S $L_{2,3}$	Cu_2S, CuS	Hybridized (Cu 3d-S 3p) states	22
[vii] XES S $L_{2,3}$	Cu_2S, CuS	Hybridized (Cu 3d -S 3p)[a] states	22
[viii] XES S L_2	Cu_2ZnSnS_4	Zn 3d-derived states [i]	
[ix] XES S L_2	Cu_2ZnSnS_4	Hybridized (Sn 5s-S 3p) states [iii]	
[x] XES S L_2	Cu_2ZnSnS_4	Hybridized (Cu 3d-S 3p)[a] states [vii]	
[xi] XAS S $L_{2,3}$	Cu_2ZnSnS_4	Hybridized (Sn 5s-S 3p)[a] states	

[a]Denotes antibonding states.

for SnS_2 these *antibonding* states are located above the valence band maximum (VBM), for SnS they (partially) lie within the valence band.[25]

Region (B) of the S $L_{2,3}$ XES spectra is very similar for the two copper sulfides and is dominated by two broad features [vi] and [vii]. Based on a comparison with DFT calculations,[22] the less-pronounced feature [vi] between 153.7 and 156.8 eV can be attributed to transitions from hybridized *bonding* Cu 3d-S 3p states, while the higher intensity feature [vii] between 157.0 and 162.3 eV can be ascribed to *antibonding* Cu 3d-S 3p states. Despite the similarity in region (B), the S $L_{2,3}$ XES spectra of the copper sulfides do significantly differ in region (A). When plotted directly on top of each other (as done in the inset of Fig. 1), it can be seen that the S 3s line of CuS [FWHM $= (4.2 \pm 0.1)$ eV] is broader than that of the Cu_2S sample [FWHM $= (3.4 \pm 0.1)$ eV]. This was observed earlier[20,29] and is possibly due to inequivalent sulfur atom positions in the CuS lattice.[29] The CuS S 3s line is also broader than the S 3s line of the CZTS samples [FWHM $= (3.4 \pm 0.1)$ eV], and thus a major contribution of a CuS impurity phase to the CZTS samples considered here is unlikely.

The spectra of the CZTS powder and thin-film sample look quite similar, and feature (A) agrees well with the shape and energetic positions of the relevant binary compounds. However, significant differences in the valence band emission (B) between CZTS and the binary compounds can be observed (Fig. 1, right). The most prominent features are found between 150.5 and 155.2 eV [region (B_1)] and between 158.2 and 162.0 eV [region (B_2)]. While the (B_1) features energetically coincide with features [i] and [iii] of the ZnS and SnS_2 and SnS emission, respectively, region (B_2) resembles feature [vii] of the copper sulfides. Note that emission [v] of the SnS reference sample also lies in that energy region, and thus it is not possible (based on these XES measurements) to derive information about the possible presence of SnS impurity phases in both CZTS samples.

In order to separate the L_2 and L_3 contributions to the XES spectra, we have used resonant excitation just below the S L_2 edge (indicated by the red arrows in Fig. 2, right), resulting in pure L_3 emission spectra (Fig. 2, left). An excitation line width of 0.17 eV, i.e., significantly less than the spin-orbit splitting, was chosen for these experiments to ensure a complete separation of the L_2 and L_3 contributions. This approach allows us to use the XES and XAS spectra, plotted on a common energy scale, to estimate the electronic band gap (see below)—when using the nonresonantly excited XES spectra, this determination would (erroneously) be based on the L_2 emission and L_3 absorption contributions. The features in the emission spectra are labeled with the same roman numerals as in Fig. 1 (right). Due to the resonant excitation, the CZTS S L_3 features in regions (B_1) and (B_2) can now be separated into individual contributions (labeled [viii]–[x]). Peak [viii] at 150.5 eV and [x] between 157.6 and 160.6 eV, are now tentatively assigned to be associated with feature [i] in the spectrum of ZnS and feature [vii] in the spectrum of Cu_2S, respectively. Hence, the top of the CZTS valence band appears to be dominated by Cu 3d-derived states, while the states ~10 eV below the VBM (i.e., at an emission energy of ~150 eV) appear to be dominated by Zn 3d-derived states. Finally, the very distinct CZTS feature [ix] at

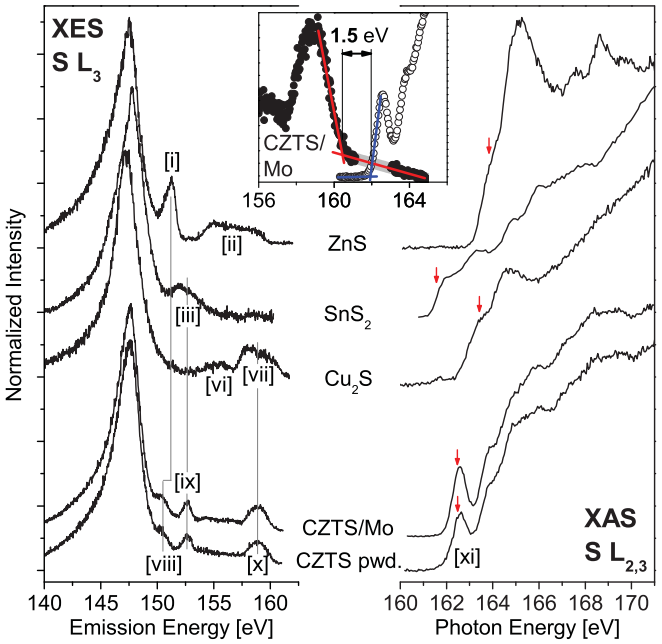

FIG. 2. (Color online) S L_3 XES (left) and S $L_{2,3}$ XAS (right) spectra of CZTS samples and related binary compounds. The red arrows at the XAS spectra indicate the resonant excitation energy used to measure the corresponding XES spectra. Inset: S L_3 XES and S $L_{2,3}$ XAS spectra of a CZTS/Mo thin film on a common energy scale. The linear extrapolations to determine the VBM and CBM positions, as well as the estimated "band gap" of 1.5 eV, are also indicated.

152.6 eV is assigned to correlate with the SnS_2 emission [iii], suggesting the influence of Sn 5s-derived states. We note that features [ix] and [x] are much narrower than the corresponding features [iii] and [vii], which is most likely due to variations in band dispersion, giving rise to a narrower feature in the (*k*-integrated) spectra. This will be discussed below, based on the calculated DOS of CZTS. Furthermore, variations in valence-hole lifetime broadening may also contribute to the differences in spectral width.

The right panel of Fig. 2 shows the S $L_{2,3}$ XAS spectra of the two CZTS samples and the binary reference compounds Cu_2S, ZnS, and SnS_2. Red arrows indicate the photon energies used to measure the resonantly excited S L_3 XES spectra in Fig. 2 (left). Both CZTS samples show a pronounced resonance [xi] at 162.6 eV and some fine structure at higher photon energies. Only the absorption spectrum of the SnS_2 reference also exhibits significant intensity at or below 162.6 eV, while the absorption edge of Cu_2S and ZnS is found at higher photon energies. This suggests that feature [xi] in the S $L_{2,3}$ XAS spectra of the CZTS samples is indicative for bands derived from Sn- and/or S-related states, which will be discussed based on the comparison with the DFT DOS results below. It should be noted that such prominent peaks directly at the absorption onset can be due to the formation of a core exciton, i.e., an electron-hole pair with a distinct core-exciton binding energy.[18,23,30–32] Absorption into the core-excitonic state would generally be expected just below the "true" absorption onset (i.e., the excitation of a core electron directly into the CBM). Thus, in absence of further information about

the presence or absence of a core exciton, the energy derived from an onset evaluation will always give a lower bound for the "true" (i.e., ground-state) CBM energy. In the present case, we believe the impact of a core exciton to be of minor importance, since we find a CZTS "band gap" value that agrees well with values determined by UV-Vis spectroscopy (see below). Also note that a careful analysis of other compound semiconductor systems (e.g., CdS[18,23]) has shown that, even in the presence of a core exciton, it is quite possible that the true CBM and the core-exciton signature incidentally overlap, in particular if the two are present in different regions of momentum space.

Based on the XES (XAS) measurements, we now use the energy of the VBM (CBM) relative to the created core hole to compute the electronic "band gap" energy. Since the "band gap" depends on the absorption onset in XAS, this "band gap" can be influenced by the potential existence of the above-mentioned core excitonic features in the XAS spectra. Hence, if a core exciton is present, our "band gap" value represents a lower bound to the ground-state band gap.[33] The inset of Fig. 2 shows the S L_3 XES and S $L_{2,3}$ XAS spectra of the CZTS/Mo thin-film sample on a common energy scale.[34] As indicated, the VBM and CBM positions were determined by linear extrapolation of the leading edges of the spectra (note that the leading edges of both spectra are due to the L_3 contribution, as discussed above). The resulting "band gap" for both CZTS samples is 1.5 (±0.3) eV, which agrees well with band-gap values determined by UV-Vis spectroscopy (1.5 eV,[2]). For the related binary compounds ZnS, SnS_2, and Cu_2S, we find "band-gap" values of 3.2 (±0.3), 1.7 (±0.4),[35] and 1.2 (±0.3) eV, respectively. The corresponding (UV-Vis) literature values are 3.7 eV for ZnS,[36] 2.1–2.3 eV for SnS_2,[37] and 1.0–1.4 eV for Cu_2S.[38] While this shows a good agreement for Cu_2S, the band gaps of ZnS and SnS_2 appear underestimated in the XES and XAS experiments, suggesting a significant contribution of core-excitonic states to the spectra of the latter two binary compounds.

In Fig. 3, a direct comparison of results from first-principles DOS calculations (1)–(4)[8,9] with experimental S L_3 XES (left) and S $L_{2,3}$ XAS (right) spectra of the CZTS/Mo thin-film sample (5) is shown. The presented CZTS DOS taken from Chen *et al.*[8] [→DOS (1)] and Paier *et al.*[9] [→DOS (2)–(4)] are based on first-principles DFT calculations using the projector augmented-wave (PAW) method[39] implemented in the VASP code.[40] DOS (1) and (2) were computed by the generalized gradient approximation (GGA) using the PW91[41] and PBE[42] functionals, respectively, and DOS (3) was calculated using the PAW routine applying the Heyd-Scuseria-Ernzerhof (HSE)[43] hybrid functional. In addition, also the results of quasiparticle calculations[44] applying the G_0W_0 method[45] are presented [DOS (4)]. Although hybrid functional and, in particular, G_0W_0 calculations have proven to yield better results than the GGA,[9] we also include the GGA PW91 DOS in the following comparative discussion, because the corresponding detailed orbital-projected partial DOS (PDOS) data is only available on the computationally less-intensive GGA level. The GGA PW91 PDOS of the Cu, Zn, Sn, and S orbitals from Ref. 8 are thus also presented in Fig. 3 [(1a)–(1d)]. The respective electronic configurations are color coded: contributions with s-, p-, and d-character are shown in red, green, and blue, respectively. Note that only the most prominent bands of

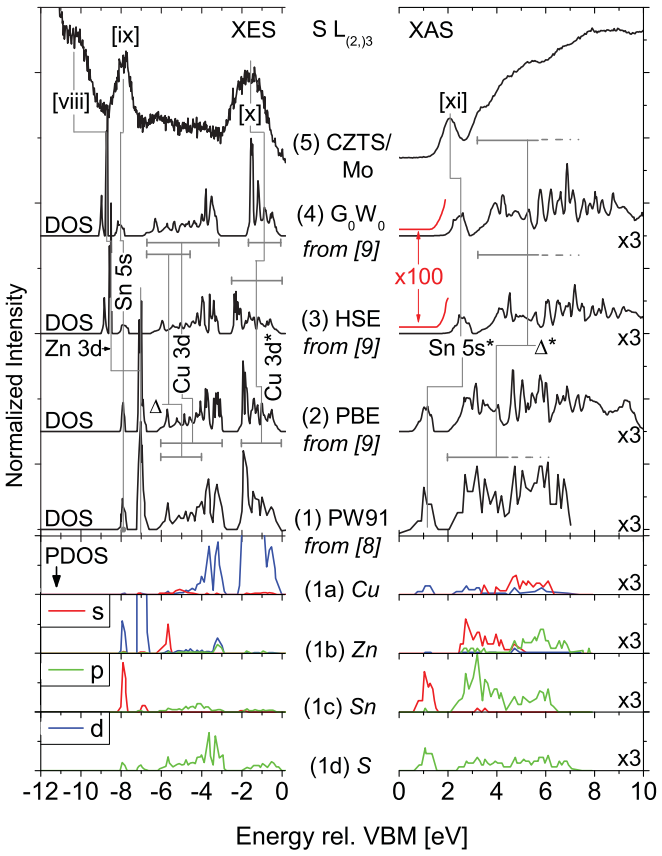

FIG. 3. (Color online) Calculated CZTS GGA DOS from Refs. 8 and 9, using (1) PW91 ("PW91") and (2) PBE ("PBE") functionals, respectively. For DOS (1) also the partial DOS [PDOS, (1a)–(1d)] is shown (Ref. 8). DOS (3) and (4) result from calculations using hybrid functionals ("HSE") (Ref. 9) and the quasiparticle approach ("G_0W_0") (Ref. 9), respectively. In addition, experimental S L_3 XES (left) and S $L_{2,3}$ XAS (right) spectra of a CZTS/Mo thin film (5) are shown for comparison. The assignment of the spectral features according to the calculated DOS is indicated. Note that the calculated conduction band DOS and its onset are magnified by a factor of 3 and 100, respectively, to allow easier comparison with the experimental data. PDOS contributions with s-, p-, and d-characters are shown in red, green, and blue, respectively, and only the most prominent bands of the respective PDOS are depicted. The vertical lines indicate the shifts of the (P)DOS contributions between different DFT calculations and related spectral features in the experimental XES/XAS data.

the respective PDOS are shown. Furthermore, the calculated conduction band (P)DOS in Fig. 3 are magnified by a factor of 3 for all calculations. The PW91 DOS and PDOS data in Fig. 3 was digitized from Ref. 8, while the DOS data from Ref. 9 was provided to us in electronic form by Paier *et al.* To enable a direct comparison between experiment and theory, the XES and XAS measurements are shown on the same energy scale as the DOS (spectra (5) in Fig. 3), i.e., the energy is given relative to the VBM. As described above, the latter was determined by linear approximation of the leading S L_3 emission edge (see inset of Fig. 2). Note that the calculations provide a ground-state description, while the correct description of experimental spectra would need to include a (dipole) operator describing the interaction of the electrons with the photon field; thus, the experimental

spectra are governed by transition matrix elements (and dipole selection rules) involving initial and final states. In consequence, while theory and experiment can be well compared in terms of band energies (relative to the VBM), the respective intensities may not be directly comparable.

Taking the well-known shortcomings of DFT calculations (in particular the difficulties to compute the correct binding energy of localized states such as Zn 3d) into account, the comparison of the S L_3 XES spectrum of the CZTS/Mo thin-film sample with the calculated G_0W_0 DOS supports our assignment of features [viii] and [x] to transitions from a narrow localized Zn 3d band and hybridized *antibonding* Cu 3d-S 3p ("Cu 3d*") states, respectively. In addition, emission [ix] can now be ascribed to transitions from hybridized *bonding* Sn 5s-S 3p ("Sn 5s") states. The earlier discussed difference in the line width of feature [ix] for CZTS and feature [iii] for SnS_2 are also reflected in the Sn PDOS of CZTS [(1c) in Fig. 3] and SnS_2 (not shown). While the DOS of CZTS indicates a very narrow Sn 5s-S 3p band,[8,9] for SnS_2 these states are found to have a significantly larger bandwidth.[25] Both, the PW91 PDOS as well as the G_0W_0 DOS, suggest an additional broadband between −6 and −3 eV consisting of hybridized *bonding* Cu 3d-S 3p ("Cu 3d") states and a linear combination of Cu 4s, Zn 4s, and Sn 5p states hybridized with *bonding* S 3p states ("Δ").[9] In contrast, the CZTS S L_3 XES spectrum shows only weak emission intensity in this energy window, which we attribute to small matrix elements for the corresponding transitions. Note that a significant fraction of the states in this region have *p*-symmetry, for which transitions into S 2p core holes are dipole forbidden.

After discussing the valence band structure, we now focus on the conduction band. Again, the calculations lead to qualitatively similar results. All DOS calculations suggest that the conduction band exhibits a well-defined narrow band that is significantly separated from the rest of the conduction band. However, compared to the GGA calculations, the HSE and G_0W_0 DOS are shifted to higher energies (i.e., away from the VBM) in better agreement with the experimental data. This observation is in accordance with the well-known difficulty of GGA calculations to compute the correct band gap, generally resulting in an underestimated value.[8,9] Closer inspection of the region of the G_0W_0 and HSE CB onset [e.g., multiplying by a factor of 100, yielding the red lines near the XAS spectra of (3) and (4) in Fig. 3], shows good agreement between the position of the CBM for the theoretical and experimental data, corresponding to a good agreement of the theoretically and experimentally derived band-gap energy (1.5 eV[8,9]). However, the main intensity of the narrow band at the CBM lies at lower energies in the experiment than in the calculation. This can most likely be explained by the presence of a core-excitonic final state in the x-ray absorption process. The higher intensity at the absorption onset in the experimental data when compared to the calculated DOS might thus be attributed to an incidental spectral overlap of core-excitonic states formed with bands above the CBM and the "true" CBM, similar to the case of CdS.[18] The comparison between calculated DOS and experimental XAS CZTS data confirms the earlier tentative assignment of the states at the bottom of the conduction band. Accordingly, feature [xi] of the S $L_{2,3}$ XAS spectrum is attributed to hybridized *antibonding* Sn 5s-S 3p states ("Sn 5s*"). The higher states of the conduction band can then be attributed to a linear combination of Cu 4s, Zn 4s, and Sn 5p orbitals, hybridized with *antibonding* S 3p states ("Δ*").

Altogether, we find a good agreement between experimental S $L_{(2,)3}$ XES and XAS data and calculated HSE and G_0W_0 DOS, with the notable exception of the energy position of the Zn 3d-derived band [viii]. Hence the previously published band structure by Paier *et al.*[9] is supported by the S $L_{(2,)3}$ XES and XAS measurements presented here. Taking the well-known shortcomings of the GGA approach into account, namely the inability to compute the correct binding energy of localized states (leading to an incorrect Zn 3d position) and a significant underestimation of the band gap (leading to an incorrect "Sn 5s*" position), also the DOS calculations of Chen *et al.*[8] give a satisfactory description.

IV. SUMMARY

We have characterized CZTS thin-film and powder samples and related binary compounds by S $L_{2,3}$ x-ray emission and absorption spectroscopy. By comparing spectra of CZTS with those of corresponding binary references and with published DFT DOS calculations, it is possible to assign the major emission and absorption features of the CZTS spectra. It was found that the top (bottom) of the CZTS valence (conduction) band is dominated by hybridized *antibonding* Cu 3d-S 3p (Sn 5s-S 3p) states. Best agreement of the experimental data with theory is found for the CZTS density of states calculated by Paier *et al.*[9] The electronic band gap in the near-surface region of the investigated CZTS materials is determined to be 1.5 (±0.3) eV, which agrees well with previously reported UV-Vis data (1.5 eV^2) and constitutes an optimal band gap for the use of CZTS in photovoltaic devices.

ACKNOWLEDGMENTS

M. Bär and R.G. Wilks acknowledge the financial support by the Impuls- und Vernetzungsfonds of the Helmholtz-Association (Grant No. VH-NG-423). The ALS is funded by the Department of Energy, Basic Energy Sciences, Contract No. DE-AC02-05CH11231. Furthermore, the authors thank J. Paier and G. Kresse for making their calculated DOS data [9] available in electronic form.

*marcus.baer@helmholtz-berlin.de

[1] T. M. Friedlmeier, H. Dittrich, and H.-W. Schock, *Ternary and Multinary Compounds. Proc. 11th Int. Conf. on Ternary and Multinary Compounds, ICTMC-11*, (Salford, UK, 1998), Vol. 152, p. 345.

[2] T. Tanaka, T. Nagatomo, D. Kawasaki, M. Nishio, Q. Guo, A. Wakahara, A. Yoshida, and H. Ogawa, J. Phys. Chem. Solids **66**, 1978 (2005).

[3] H. Katagiri, K. Jimbo, S. Yamada, T. Kamimura, W. S. Maw, T. Fukano, T. Ito, and T. Motohiro, Appl. Phys. Express **1**, 041201 (2008).

[4] A. Weber, H. Krauth, S. Perlt, B. Schubert, I. Kötschau, S. Schorr, and H.-W. Schock, Thin Solid Films **517**, 2524 (2009).

[5] J. J. Scragg, D. M. Berg, and P. J. Dale, J. Electroanal. Chem. **646**, 52 (2010).

[6]G. S. Babu, Y. K. Kumar, P. U. Bhaskar, and V. S. Raja, Semicond. Sci. Technol. **23**, 085023 (2008); Sol. Energy Mater. Sol. Cells **94**, 221 (2010).
[7]T. K. Todorov, K. B. Reuter, and D. B. Mitzi, Adv. Mater. **22**, 1 (2010).
[8]S. Chen, X. G. Gong, A. Walsh, and S.-H. Wei, Appl. Phys. Lett. **94**, 041903 (2009).
[9]J. Paier, R. Asahi, A. Nagoya, and G. Kresse, Phys. Rev. B **79**, 115126 (2009).
[10]M. Ichimura and Y. Nakashima, Jpn. J. Appl. Phys. **48**, 090202 (2009).
[11]C. Persson, J. Appl. Phys. **107**, 053710 (2010).
[12]G. Moh, Chem. Erde **34**, 1 (1975).
[13]I. D. Olekseyuk, I. V. Dudchak, and L. V. Piskach, J. Alloys Compd. **368**, 135 (2004).
[14]S. Schorr, A. Weber, V. Honkimäki, and H.-W. Schock, Thin Solid Films **517**, 2461 (2009); S. Schorr, Sol. Energy Mater. Sol. Cells, doi:10.1016/j.solmat.2011.01.002 (2011).
[15]B.-A. Schubert, B. Marsen, S. Cinque, T. Unold, R. Klenk, S. Schorr, and H.-W. Schock, Prog. Photovolt: Res. Appl. **19**, 93 (2011).
[16]A. Meisel, G. Leonhardt, and R. Szargan, *X-Ray Spectra and Chemical Binding* (Springer, Berlin, 1989), Springer Series in Chemical Physics Vol. 37.
[17]J. J. Jia, T. A. Callcott, J. Yurkas, A. W. Ellis, F. J. Himpsel, M. G. Samant, J. Stoehr, D. L. Ederer, J. A. Carlisle, E. A. Hudson, L. J. Terminello, D. K. Shuh, and R. C. C. Perera, Rev. Sci. Instrum. **66**, 1394 (1995).
[18]L. Weinhardt, O. Fuchs, E. Umbach, C. Heske, A. Fleszar, W. Hanke, and J. D. Denlinger, Phys. Rev. B **75**, 165207 (2007).
[19]Calculated using attenuation lengths from B. L. Henke, E. M. Gullikson, and J. C. Davis, At. Data Nucl. Data Tables **54**, 181 (1993); [http://wwwcxro.lbl.gov/optical_constants/atten2.html].
[20]C. Heske, U. Groh, O. Fuchs, E. Umbach, N. Franco, C. Bostedt, L. J. Terminello, R. C. C. Perera, K. H. Hallmeier, A. Preobrajenski, R. Szargan, S. Zweigart, W. Riedl, and F. Karg, Phys. Stat. Sol. **187**, 13 (2001).
[21]National Institute of Standards and Technology, NIST X-Ray Photoelectron Spectroscopy Database, Version 3.5, [http://srdata.nist.gov/xps/].
[22]N. S. Pavlov, V. A. Galkin, I. A. Nekrasov, and E. Z. Kurmaev, Phys. Solid State **51**, 2207 (2009).
[23]L. Weinhardt, O. Fuchs, A. Fleszar, M. Bär, M. Blum, M. Weigand, J. D. Denlinger, W. Yang, W. Hanke, E. Umbach, and C. Heske, Phys. Rev. B **79**,165305 (2009).
[24]L. Zhou, T. A. Callcott, J. J. Jia, D. L. Ederer, and R. Perera, Phys. Rev. B **55,** 5051 (1997).
[25]I. Lefebvre, M. Lannoo, J. Olivier-Fourcade, and J. C. Jumas, Phys. Rev. B **44**, 1004 (1991).
[26]A. Walsh and G. W. Watson, J. Phys. Chem. B **109**, 18868 (2005).
[27]A. Gheorghiude la Rocque, E. Belin-Ferré, M. F. Fontaine, C. Senemaud, J. Olivier-Fourcade, and J. C. Jumas, Philos. Mag. B **80**, 1933 (2000).
[28]I. Lefebvre-Devos, J. Olivier-Fourcade, J. C. Jumas, and P. Lavela, Phys. Rev. B **61**, 3110 (2000).
[29]E. Z. Kurmaev, J. van Ek, D. L. Ederer, L. Zhou, T. A. Callcott, R. C. C. Perera, V. M. Cherkashenko, S. N. Shamin, V. A. Trofimova, S. Bartkowski, M. Neumann, A. Fujimori, and V. P. Moloshag, J. Phys. Condens. Matter **10**, 1687 (1998).
[30]J. Lüning, J.-E. Rubensson, C. Ellmers, S. Eisebitt, and W. Eberhardt, Phys. Rev. B **56**, 13147 (1997).
[31]B. Gilbert, B. H. Frazer, H. Zhang, F. Huang, J. F. Banfield, D. Haskel, J. C. Lang, G. Srajer, and G. De Stasio, Phys. Rev. B **66**, 245205 (2002).
[32]D. Eich, O. Fuchs, U. Groh, L. Weinhardt, R. Fink, E. Umbach, C. Heske, A. Fleszar, W. Hanke, E. Gross, C. Bostedt, T. v. Buuren, N. Franco, and L. J. Terminello, M. Keim, G. Reuscher, H. Lugauer, and A. Waag, Phys. Rev. B **73**, 115212 (2006).
[33]M. Bär, S. Nishiwaki, L. Weinhardt, S. Pookpanratana, O. Fuchs, M. Blum, W. Yang, J. D. Denlinger, W. N. Shafarman, and C. Heske, Appl. Phys. Lett. **93**, 244103 (2008).
[34]The region of the S L_3 XES spectrum shown in grey represents a linear fit of the background after removal of the (intense) Rayleigh line.
[35]Because of the low signal-to-noise ratio of the resonantly excited SnS_2 spectrum, which prevents an accurate extrapolation of the VBM position, we have used the nonresonantly excited S $L_{2,3}$ XES spectrum to determine the S L_2 VBM position in this case. This value was then corrected by the S 2p spin-orbit splitting of 1.2 eV to derive the position of the S L_3 VBM.
[36]A. Goldmann and E.-E. Koch, Editors, Volumes III/23a: T. C. Chiang and F. J. Himpsel, 2.1.22 ZnS, SpringerMaterials - The Landolt-Börnstein Database [http://www.springermaterials.com].
[37]O. Madelung, U. Rössler, and M. Schulz, Editors, Volumes III/17E-17F-41C: *Tin Disulfide (SnS_2) Band Structure, Energy Gaps*. SpringerMaterials—The Landolt-Börnstein Database [http://www.springermaterials.com], doi: 10.1007/10681727_785.
[38]O. Madelung, U. Rössler, and M. Schulz, Editors, Volumes III/17E-17F-41C: *Copper Sulfides (Cu_2S, $Cu_{(2x)}S$) Energy Gap, Effective Masses*. Springer Materials—The Landolt-Börnstein Database (http://www.springermaterials.com), doi: 10.1007/10681727_71.
[39]P. E. Blöchl, Phys. Rev. B **50**, 17953 (1994). G. Kresse and D. Joubert, *ibid.* **59**, 1758 (1999).
[40]G. Kresse and J. Hafner, Phys. Rev. B Phys. Rev. B **48**, 13115 (1993); G. Kresse and J. Furthmüller, Comput. Mater. Sci. **6**, 15 (1996); **54**, 11169 (1996).
[41]J. P. Perdew and Y. Wang, Phys. Rev. B **45**, 13244 (1992).
[42]J. P. Perdew, K. Burke, and M. Ernzerhof, Phys. Rev. Lett. **77**, 3865 (1996).
[43]J. Heyd, G. E. Scuseria, and M. Ernzerhof, J. Chem. Phys. **118**, 8207 (2003).
[44]M. Shishkin and G. Kresse, Phys. Rev. B **74**, 035101 (2006); **75**, 235102 (2007); F. Fuchs, J. Furthmüller, F. Bechstedt, M. Shishkin, and G. Kresse, *ibid.* **76**, 115109 (2007).
[45]L. Hedin, Phys. Rev. **139**, A796 (1965).